Signal Processing 148 (2018) 48–55

Contents lists available at ScienceDirect

Signal Processing

journal homepage: www.elsevier.com/locate/sigpro

Real-valued DOA estimation with unknown number of sources via reweighted nuclear norm minimization

Fenggang Sun[a,c], Qihui Wu[b], Peng Lan[a,*], Guoru Ding[c], Lizhen Chen[a]

[a] College of Information Science and Engineering, Shandong Agricultural University, Tai'an 271018, China
[b] College of Electronic and Information Engineering, Nanjing University of Aeronautics and Astronautics, Nanjing 211106, China
[c] College of Communications Engineering, PLA University of Science and Technology, Nanjing 210007, China

ARTICLE INFO

Article history:
Received 16 May 2017
Revised 9 February 2018
Accepted 12 February 2018
Available online 13 February 2018

Keywords:
DOA estimation
Non-uniform linear array
Spatial smoothing MUSIC
Reweighted nuclear norm minimization

ABSTRACT

Traditional MUSIC-like methods for direction-of-arrival (DOA) estimation require the number of sources *a priori* and suffer from the heavy computational burden caused by complex-valued operations and exhaustive spectral search. In this paper, we propose two novel real-valued estimation methods without knowing the number of sources to overcome these weaknesses. Specifically, we first transform the complex-valued second-order statistics (covariance matrix) into real-valued one by unitary transformation and taking its real (or imaginary) part, respectively. We then formulate a real-valued low rank recovery problem to reveal the relation between the real-valued covariance matrices and source number. Finally, we propose a computationally efficient approach to solve the optimization problem via reweighted nuclear norm minimization. Simulation results show that without knowing the number of sources, the proposed methods exhibit superior estimation performance and can substantially reduce the complexity, as compared to the state-of-the-art techniques.

1. Introduction

Direction-of-arrival (DOA) estimation is an important topic in radar, sonar, wireless communications and other applications [1]. Various high- and super-resolution estimation techniques have been widely used, such as Capon's estimator [2], multiple signal classification (MUSIC) [3], estimation of signal parameters via rotational invariance technique (ESPRIT) [4], and root-MUSIC [5]. In general, these methods can resolve at most $N-1$ sources for an N-element uniform linear array (ULA). To detect more sources than physical sensors, non-uniform linear array geometries for underdetermined DOA estimation have received considerable interest in recent years, such as minimum redundancy array (MRA) [6], coprime array[7,8], nested array [9,10] and nested MRA [11]. These non-uniform arrays can achieve more degrees-of-freedom (DOFs). Specifically, by utilizing the second-order statistics (covariance) of the received data, the nested array [9] can identify $\mathcal{O}(M^2)$ sources with M physical sensors, while the nested MRA [11] is capable of identifying $\mathcal{O}(M^2N^2)$ sources with MN physical sensors.

The information of source number is essential for accurate DOA estimation. However, the source number information can hardly be obtained correctly due to the effect of medium or noise characteristics, which may deteriorate the estimation accuracy. Therefore, the problem in hand is to estimate sources DOAs with increased detectable capability (detecting more sources) while the source number is kept unknown. To this end, two main representative approaches have been proposed. The first approach [12,13] is to use a low rank matrix denoising (LRD) approach to estimate the number of sources, and the following MUSIC-like subspace method is used to estimate DOAs. The second approach [14,15] uses sparsity-based recovery by assuming a sparse representation of the incident DOAs that lie on the pre-specified discrete grid. Due to exhaustive spectral search and frequent complex-valued operations, the former suffers from the heavy computation burden, especially when the sensor array is large [12]. Meanwhile, the latter suffers from the off grid problem, since the true DOAs are unlikely to lie on the pre-specified grid exactly.

In this paper, we study the computationally efficient real-valued DOA estimation approaches without knowing the number of sources. Firstly, we transform the complex-valued covariance matrix to real-valued ones from two perspectives, i.e., taking the real (or imaginary) part [16] and unitary transformation [17], which helps to reduce the computation burden. Secondly, we reveal the relations between the two real-valued covariance matrices and source number, and then formulate a real-valued low rank recovery problem to acquire the number of sources. Then, we propose a computationally efficient reweighted nuclear

* Corresponding author.
E-mail address: lanpeng@sdau.edu.cn (P. Lan).

https://doi.org/10.1016/j.sigpro.2018.02.014
0165-1684/

norm minimization approach to solve the optimization problem. Finally, we obtain the real-valued noise subspace through singular value decomposition (SVD) and estimate the DOAs through real-valued MUSIC. In-depth simulation results show that the proposed approaches can estimate underdetermined DOAs with less sensors, and exhibits superior estimation performance but with substantially reduced complexity, as compared to the state-of-the-art methods.

Notations: Throughout the paper, we use the lowercase (uppercase) boldface symbols to represent vectors (matrices). $(\cdot)^*$, $(\cdot)^T$, and $(\cdot)^H$ denote conjugate, transpose, and conjugate transpose, respectively. $\mathbf{I}_M$ and $\mathbf{J}_M$ are $M\times M$ identity and reverse identity matrices, respectively. $\|\mathbf{A}\|_*$, $\|\mathbf{A}\|_F$, and $\sigma_m(\mathbf{A})$ denote the nuclear norm, Frobenius norm, and the mth singular value of $\mathbf{A}$, respectively. $\lceil\cdot\rceil$ denotes the round up to integer operation. $\mathrm{Re}(\cdot)$ takes the real part. $\mathrm{tr}(\cdot)$ denotes the trace operation.

2. System model

Consider a linear sensor array with M sensors which are non-uniformly located. Suppose $l_i = z_i\lambda/2, i = 1, 2, \ldots, M$ denotes the location of the ith sensor from the origin of reference, where z_i is an integer and λ is the wavelength. There are K uncorrelated narrowband sources from directions $\boldsymbol{\Theta} = [\theta_1, \theta_2, \ldots, \theta_K]$ simultaneously impinging on the array. Therefore, the data collected by all the sensors at time $t(1 \le t \le T)$ can be expressed as

$$\mathbf{x}(t) = \sum_{k=1}^{K} \mathbf{a}(\theta_k)s_k(t) + \mathbf{n}(t) = \mathbf{A}\mathbf{s}(t) + \mathbf{n}(t). \tag{1}$$

Here $\mathbf{A}=[\mathbf{a}(\theta_1), \mathbf{a}(\theta_2), \ldots, \mathbf{a}(\theta_K)]$ is the array manifold matrix, and $\mathbf{a}(\theta_k)$ is the $M\times 1$ steering vector with its ith element taken as $e^{j\pi z_i \sin\theta_k}$. $\mathbf{s}(t) = [s_1(t), s_2(t), \ldots, s_K(t)]^T$ is the source signal vector. $\mathbf{n}(t)$ denotes the additive white noise with power σ^2, which is uncorrelated with $\mathbf{s}(t)$.

The covariance matrix of the data vector $\mathbf{x}(t)$ is obtained as

$$\mathbf{R}_{xx} = \mathrm{E}\left[\mathbf{x}(t)\mathbf{x}^H(t)\right] = \mathbf{A}\mathbf{R}_{ss}\mathbf{A}^H + \sigma^2\mathbf{I}_M, \tag{2}$$

where $\mathbf{R}_{ss} = \mathrm{E}\left[\mathbf{s}(t)\mathbf{s}^H(t)\right] = \mathrm{diag}\left(\left[\sigma_1^2, \sigma_2^2, \ldots, \sigma_K^2\right]\right)$ is the source covariance matrix. In practice, the covariance matrix is estimated by using the T available samples, i.e.,

$$\widehat{\mathbf{R}}_{xx} = \frac{1}{T}\sum_{t=1}^{T}\mathbf{x}(t)\mathbf{x}^H(t). \tag{3}$$

Vectorizing the covariance matrix $\mathbf{R}_{xx}$ (or its estimate $\widehat{\mathbf{R}}_{xx}$), we can obtain a virtual difference co-array with larger aperture to achieve higher DOFs [7,18]. By applying spatial smoothing to the consecutive elements of the co-array, a virtual M_{ca}-element ULA is formed and the corresponding covariance matrix is denoted as

$$\mathbf{R}_{sm} = \mathbf{A}_{ca}\mathbf{R}_{ss}\mathbf{A}_{ca}^H + \sigma^2\mathbf{I}_{M_{ca}}, \tag{4}$$

where $\mathbf{A}_{ca}=[\mathbf{a}_{ca}(\theta_1), \mathbf{a}_{ca}(\theta_2), \ldots, \mathbf{a}_{ca}(\theta_K)]$ is the manifold matrix of the virtual ULA, and $\mathbf{a}_{ca}(\theta_k)$ is the $M_{ca}\times 1$ steering vector with the ith element being $e^{j\pi i \sin\theta_k}, i = 1, 2, \ldots, M_{ca}$.

In general, $M_{ca} > M$ holds [7,9,11], implying that as compared to the original array, the virtual ULA has more sensor elements and can detect more sources. It is noted that as long as the source number K is less than the sensor number of the virtual ULA M_{ca}, the noise-free covariance matrix $\mathbf{R}_{sig} = \mathbf{R}_{sm} - \sigma^2\mathbf{I} = \mathbf{A}_{ca}\mathbf{R}_{ss}\mathbf{A}_{ca}^H$ in Eq. (4) is low-rank (rank K), which can be utilized to estimate the number of sources.

3. Proposed algorithms

According to Pal and Vaidyanathan [7], given the source number K *a priori*, the DOAs are estimated by finding the K maxima of its MUSIC spectrum. Without this priori information, the source number can be revealed as a byproduct via low rank matrix denoising [12]. However, these methods suffer from the heavy computation burden caused by complex-valued computations. To the end, we study the real-valued versions for DOA estimation to reduce the complexity without knowing the source number *a priori*.

3.1. Real-valued transformation

In this section, we first transform the complex-valued covariance matrix to real-valued ones from two perspectives and then reveal the relations between the real-valued matrices and the source number.

3.1.1. Real part of covariance matrix (RPCM)

Let $\mathbf{R}_{rv}^{(1)}$ denote the real part of $\mathbf{R}_{sm}$, i.e., $\mathbf{R}_{rv}^{(1)} = \mathrm{Re}(\mathbf{R}_{sm}) = \frac{1}{2}(\mathbf{R}_{sm} + \mathbf{R}_{sm}^*)$. As the noise-free matrix $\mathbf{R}_{sig}$ of $\mathbf{R}_{sm}$ is low rank, the noise-free matrix of $\mathbf{R}_{rv}^{(1)}$ is still low rank. Since $\mathbf{R}_{rv}^{(1)}$ is a symmetrical real-valued matrix, its SVD only requires real-valued computation, denoted as

$$\mathbf{R}_{rv}^{(1)} = \mathbf{U}^{(1)}\boldsymbol{\Sigma}^{(1)}{\mathbf{V}^{(1)}}^T = \mathbf{U}_s^{(1)}\boldsymbol{\Sigma}_s^{(1)}\mathbf{V}_s^{(1)T} + \mathbf{U}_n^{(1)}\boldsymbol{\Sigma}_n^{(1)}\mathbf{V}_n^{(1)T}, \tag{5}$$

where the subscripts s and n denote the signal- and noise- subspace, respectively, and $\boldsymbol{\Sigma}_s^{(1)}$ and $\boldsymbol{\Sigma}_n^{(1)}$ are two diagonal matrices containing the real valued significant- and zero- singular values, respectively.

According to Yan et al. [16], the noise subspace spanned by $\mathbf{V}_n^{(1)}$ is simultaneously orthogonal to the virtual steering vectors at true DOAs and their mirror directions, i.e., if $\theta \in \boldsymbol{\Theta}$, the following constraint holds,

$$\begin{cases} \mathrm{span}\left(\mathbf{V}_n^{(1)}\right) \perp \mathrm{span}(\mathbf{a}_{ca}(\theta)), \\ \mathrm{span}\left(\mathbf{V}_n^{(1)}\right) \perp \mathrm{span}(\mathbf{a}_{ca}(-\theta)). \end{cases} \tag{6}$$

The dual orthogonality (6) will cause mirror ambiguity, which doubles the number of candidate DOAs that satisfy (6). However, this property can also be utilized to halve the angular field for spectral search and reduce the complexity as a result.

Let P denote the number of non-zero DOAs that their mirror angles also belong to $\boldsymbol{\Theta}$, which is an even integer. If $0^\circ \notin \boldsymbol{\Theta}$, the number of candidate DOAs is $2K - P$. While if $0^\circ \in \boldsymbol{\Theta}$, the number becomes $2K - P - 1$. In general, the K incident DOAs are randomly distributed in the region $[-\pi/2, \pi/2]$. The event that both an angle and its mirror angle belong to $\boldsymbol{\Theta}$ is usually a small probability event. Similarly, the event $0^\circ \in \boldsymbol{\Theta}$ is also a small probability event. Consequently, in most cases, the number of candidate DOAs is $2K$. As long as $2K$ is less than the number of the virtual ULA M_{ca}, the noise-free matrix of $\mathbf{R}_{rv}^{(1)}$ is low-rank.

Due to dual orthogonality, it is noted that for the real-valued noise-free covariance matrix $\mathbf{R}_{rv}^{(1)}$, $2K < M_{ca}$ should hold, while for its complex version, $K < M_{ca}$ holds. Thus, the number of detectable sources is decreased. However, we will show that this decrease can significantly reduce the computational complexity.

Remark 1. Except for the real part of the covariance matrix, the imaginary part of the covariance matrix (IPCM) can also span the same real-valued noise subspace via SVD [16] as RPCM, implying that IPCM can achieve the same relation between real-valued matrix and source number as RPCM. Without loss of generality, we only consider the RPCM case in this paper.

3.1.2. Unitary transformation of covariance matrix (UTCM)

The covariance matrix in Eq. (4) can be transformed to a real-valued one by unitary transformation [19]. The unitary transformation matrix is defined as

$$\mathbf{Q}_{2q} = \frac{1}{\sqrt{2}}\begin{bmatrix} \mathbf{I}_q & \mathbf{J}_q \\ j\mathbf{J}_q & -j\mathbf{I}_q \end{bmatrix}, \tag{7}$$

$$\mathbf{Q}_{2q+1} = \frac{1}{\sqrt{2}}\begin{bmatrix} \mathbf{I}_q & \mathbf{0}_{q\times 1} & \mathbf{J}_q \\ \mathbf{0}_{1\times q} & \sqrt{2} & \mathbf{0}_{1\times q} \\ j\mathbf{J}_q & \mathbf{0}_{q\times 1} & -j\mathbf{I}_q \end{bmatrix}, \tag{8}$$

where q is an positive integer. Then we are able to form a real symmetric transformed covariance matrix [17], denoted by $\mathbf{R}_{rv}^{(2)}$ as

$$\mathbf{R}_{rv}^{(2)} = \mathrm{Re}\left(\mathbf{Q}_{M_{ca}}\mathbf{R}_{sm}\mathbf{Q}_{M_{ca}}^{H}\right). \tag{9}$$

Since $\mathbf{R}_{rv}^{(2)}$ is real-valued symmetrical, its SVD only requires real-valued computations, i.e.,

$$\mathbf{R}_{rv}^{(2)} = \mathbf{U}^{(2)}\mathbf{\Sigma}^{(2)}\mathbf{V}^{(2)T} = \mathbf{U}_s^{(2)}\mathbf{\Sigma}_s^{(2)}\mathbf{V}_s^{(1)T} + \mathbf{U}_n^{(2)}\mathbf{\Sigma}_n^{(2)}\mathbf{V}_n^{(2)T}, \tag{10}$$

where the subscripts s and n denote the signal- and noise-subspace, respectively.

Notice that the unitary transformation matrix $\mathbf{Q}_{Mca}$ is full rank and the rank of the noise-free matrix $\mathbf{R}_{sig}$ reveals the source number, therefore, the rank of the noise-free matrix of $\mathbf{R}_{rv}^{(2)}$ is also the number of sources.

3.2. Real-valued low rank matrix recovery

The real-valued matrices $\mathbf{R}_{rv}^{(1)}$ and $\mathbf{R}_{rv}^{(2)}$ are generated from the complex-valued covariance matrix $\mathbf{R}_{sm}$, both of which are related to the number of sources. For convenience, we use $\mathbf{R}_{rv}$ to represent $\mathbf{R}_{rv}^{(1)}$ and $\mathbf{R}_{rv}^{(2)}$. The rank of the noise-free matrix of $\mathbf{R}_{rv}$ is the number of sources if $\mathbf{R}_{rv} = \mathbf{R}_{rv}^{(2)}$, and the rank reveals the number of sources and their mirrors if $\mathbf{R}_{rv} = \mathbf{R}_{rv}^{(1)}$. Therefore, it is intuitive to recover the matrix by rank minimization. However, it is challenging due to the discrete nature of rank minimization. A feasible method is replacing the rank function with the nuclear norm, as the nuclear norm minimization is the tightest convex relaxation of the rank minimization problem. Thus we have

$$\begin{aligned} \min_{\mathbf{R}} \quad & \|\mathbf{R}\|_* \\ \text{s.t.} \quad & \|\mathbf{R}_{rv} - \mathbf{R}\|_F^2 \le \xi, \end{aligned} \tag{11}$$

where $\mathbf{R}$ is a real-valued matrix to be recovered. The optimization problem (11) is equivalent to

$$\min_{\mathbf{R}} \quad \eta\|\mathbf{R}\|_* + \frac{1}{2}\|\mathbf{R}_{rv} - \mathbf{R}\|_F^2, \tag{12}$$

where η is the regularization parameter.

3.3. Reweighted nuclear norm minimization

Since the nuclear norm minimization requires more measurements for exact recovery of the low rank solution [20], alternatively it can be replaced by Schatten p-norm, which is defined as

$$\|\mathbf{R}\|_p \triangleq \left(\sum_{m=1}^{M_{ca}} \sigma_m(\mathbf{R})^p\right)^{1/p}. \tag{13}$$

The original problem (12) can then be reformulated as

$$\min_{\mathbf{R}} \quad f_0(\mathbf{R}) = \eta p\|\mathbf{R}\|_p + \frac{1}{2}\|\mathbf{R}_{rv} - \mathbf{R}\|_F^2. \tag{14}$$

The above problem is nonconvex when $0 < p < 1$. It can be further approximated by

$$\min_{\mathbf{R}} \quad f(\mathbf{R}) = \eta p\|\mathbf{R}\|_{p,\varepsilon}^p + \frac{1}{2}\|\mathbf{R}_{rv} - \mathbf{R}\|_F^2, \tag{15}$$

where $\|\mathbf{R}\|_{p,\varepsilon} = \left(\sum_{m=1}^{M_{ca}} (\sigma_m(\mathbf{R}) + \varepsilon)^p\right)^{1/p}$ and $\varepsilon > 0$.

Instead of minimizing (15) directly, we use a reweighted auxiliary function [20] to further approximate (15), defined as

$$h(\mathbf{R}, \mathbf{w}) = \frac{1}{2}\|\mathbf{R}_{rv} - \mathbf{R}\|_F^2 + \eta\sum_{m=1}^{M_{ca}}\left(pw_m(\sigma_m(\mathbf{R}) + \varepsilon) + (1-p)w_m^{p/(p-1)}\right), \tag{16}$$

with $\mathbf{w} = [w_1, w_2, \ldots, w_{M_{ca}}]^T \ge 0$.

We then utilize a two-step iterative approach to minimize (16), specifically,

Step 1: Given $\mathbf{R}^{(k)}$ fixed at the kth iteration, $w_m^{(k)} = \left(\sigma_m\left(\mathbf{R}^{(k)}\right) + \varepsilon\right)^{p-1} > 0$ is the optimal solution of the following problem,

$$\min_{w_m} \quad pw_m\left(\sigma_m\left(\mathbf{R}^{(k)}\right) + \varepsilon\right) + (1-p)w_m^{p/(p-1)}, \tag{17}$$

which implies that $w_m^{(k)}$ is also the optimal solution to minimize $h(\mathbf{R}, \mathbf{w})$. By substituting $w_m^{(k)}$ into $h(\mathbf{R}, \mathbf{w})$, we have

$$\begin{aligned} h\left(\mathbf{R}, \mathbf{w}^{(k)}\right) &= \eta\sum_{m=1}^{M_{ca}}(\sigma_m(\mathbf{R}) + \varepsilon)^p + \frac{1}{2}\|\mathbf{R}_{rv} - \mathbf{R}\|_F^2 \\ &\ge \eta p\sum_{m=1}^{M_{ca}}(\sigma_m(\mathbf{R}) + \varepsilon)^p + \frac{1}{2}\|\mathbf{R}_{rv} - \mathbf{R}\|_F^2 \\ &= f(\mathbf{R}). \end{aligned} \tag{18}$$

Then the inequalities $h(\mathbf{R}, \mathbf{w}^{(k)}) \ge f(\mathbf{R}) \ge f_0(\mathbf{R})$ hold. To obtain the optimal solution to minimize $f_0(\mathbf{R})$, we resort to minimize $h(\mathbf{R}, \mathbf{w}^{(k)})$ alternatively.

Step 2: For fixed $\mathbf{w}^{(k)}$, to minimize $h(\mathbf{R}, \mathbf{w}^{(k)})$ is equivalent to

$$\min_{\mathbf{R}} \eta p\sum_{m=1}^{M_{ca}}\left(w_m^{(k)}\sigma_m(\mathbf{R})\right) + \frac{1}{2}\|\mathbf{R}_{rv} - \mathbf{R}\|_F^2. \tag{19}$$

Since $\mathbf{R}_{rv}$ is real-valued and symmetric, its SVD is denoted as $\mathbf{R}_{rv}$=$\mathbf{U}\mathbf{\Sigma}\mathbf{V}^T$. The singular values vector of $\mathbf{R}_{rv}$ is $\boldsymbol{\sigma}(\mathbf{R}_{rv}) = diag(\mathbf{\Sigma})$. Let $\boldsymbol{\sigma} = \boldsymbol{\sigma}(\mathbf{R}) = \left[\sigma_1, \sigma_2, \ldots, \sigma_{M_{ca}}\right]^T$ denote the singular value vector of $\mathbf{R}$. As the first term of the problem (19) only depends on the singular values of $\mathbf{R}$, (19) can be equivalently written as

$$\min_{\boldsymbol{\sigma}:\sigma_1,\sigma_2,\ldots,\sigma_{M_{ca}}\ge 0}\left\{\min_{\mathbf{R}\in R, \boldsymbol{\sigma}(\mathbf{R})=\boldsymbol{\sigma}} \eta p\sum_{m=1}^{M_{ca}}\left(w_m^{(k)}\sigma_m(\mathbf{R})\right) + \frac{1}{2}\|\mathbf{R}_{rv} - \mathbf{R}\|_F^2\right\}. \tag{20}$$

The second term $\|\mathbf{R}_{rv} - \mathbf{R}\|_F^2$ of (19) can be converted as

$$\begin{aligned} \|\mathbf{R}_{rv} - \mathbf{R}\|_F^2 &= \mathrm{tr}\left(\mathbf{R}_{rv}\mathbf{R}_{rv}^T\right) + \mathrm{tr}\left(\mathbf{R}\mathbf{R}^T\right) - 2\mathrm{tr}\left(\mathbf{R}_{rv}\mathbf{R}^T\right) \\ &= \sum_{m=1}^{M_{ca}}\sigma_m^2(\mathbf{R}_{rv}) + \sum_{m=1}^{M_{ca}}\sigma_m^2(\mathbf{R}) - 2\mathrm{tr}\left(\mathbf{R}_{rv}\mathbf{R}^T\right). \end{aligned} \tag{21}$$

According to Von Neumann's trace inequality [21], $\mathrm{tr}(\mathbf{R}_{rv}\mathbf{R}^T) \le \boldsymbol{\sigma}(\mathbf{R}_{rv})^T\boldsymbol{\sigma}(\mathbf{R})$ holds. The above inequality turns out to be equality when $\mathbf{R}$=$\mathbf{U}diag(\boldsymbol{\sigma}(\mathbf{R}))\mathbf{V}^T$. Then the optimization problem (20) reduces to

$$\min_{\boldsymbol{\sigma}:\sigma_1,\sigma_2,\ldots,\sigma_{M_{ca}}\ge 0}\left\{\sum_{m=1}^{M_{ca}}\left[\frac{1}{2}\sigma_m^2(\mathbf{R}) - \left(\sigma_m(\mathbf{R}_{rv}) - np\omega_m^{(k)}\right)\sigma_m(\mathbf{R})\right]\right\}. \tag{22}$$

As the objective function in (22) is convex and quadratic with variables $\sigma_m(\mathbf{R}_{rv})$, it has the unique global optimal solution. Considering the non-negativity of singular value, the optimal solution

for the problem (22) is

$$\sigma_m(\mathbf{R}) = \left(\sigma_m(\mathbf{R}_{rv}) - np\omega_m^{(k)}\right)^+, \tag{23}$$

where $(\cdot)^+ = \max(\cdot, 0)$.

Finally, the optimal solution of (19) is

$$\mathbf{R}^{(k+1)} = \mathbf{U}diag\left\{\left(\sigma_m(\mathbf{R}_{rv}) - \eta pw_m^{(k)}\right)^+\right\}\mathbf{V}^T. \tag{24}$$

Substituting $\mathbf{R}^{(k+1)}$ into (16), the optimization problem is converted into (17), and the optimal solution is $w_m^{(k+1)} = \left(\sigma_m\left(\widehat{\mathbf{R}}^{(k+1)}\right) + \varepsilon\right)^{p-1}$.

We see that the optimization problem is solved in a gradual and interweaved manner, which ensures the algorithm gradually converge to recover the true $\mathbf{R}_{rv}$. In addition, from (16) we can see that if ε decreases, $h(\mathbf{R}, \mathbf{w})$ will decrease. Therefore, instead of a constant ε, we can use a monotonically decreasing sequence $\{\varepsilon^{(k)}\}$, say, $\varepsilon^{(k)} = \rho\varepsilon^{(k-1)}$, $0 < \rho < 1$. Finally, we can obtain the optimal solution $\mathbf{R}^{opt}$.

3.3.1. Convergence analysis

We now analyze the convergence of the reweighted nuclear norm minimization algorithm.

Consider the $(k+1)$th iteration, after solving (17) and (19), we have

$$h\left(\mathbf{R}^{(k+1)}, \mathbf{w}^{(k+1)}\right) \le h\left(\mathbf{R}^{(k)}, \mathbf{w}^{(k+1)}\right) \le h\left(\mathbf{R}^{(k)}, \mathbf{w}^{(k)}\right). \tag{25}$$

According to (18), we have

$$f\left(\mathbf{R}^{(k+1)}, \varepsilon^{(k)}\right) \le f\left(\mathbf{R}^{(k)}, \varepsilon^{(k)}\right). \tag{26}$$

Due to the descending property of the sequence $\{\varepsilon^{(k)}\}$, the inequality

$$f\left(\mathbf{R}^{(k+1)}, \varepsilon^{(k+1)}\right) \le f\left(\mathbf{R}^{(k+1)}, \varepsilon^{(k)}\right), \tag{27}$$

holds. Therefore, the update of $\mathbf{R}$, $\mathbf{w}$, and ε will generate a non-increasing sequence of $f(\mathbf{R}, \varepsilon)$. Considering that $f(\mathbf{R}, \varepsilon) \ge f_0(\mathbf{R})$ holds and $f_0(\mathbf{R})$ is bounded below, we can conclude that the proposed algorithm will generate a non-increasing sequence of $f_0(\mathbf{R})$. Moreover, as proved in [20], the reweighting nuclear norm minimization scheme in which the proposed algorithm belongs to, can lead to stationary points of $f(\mathbf{R}, \varepsilon)$, which are the global minima in case that $p = 1$.

3.4. Real-valued MUSIC-based DOA estimation methods

The solution $\mathbf{R}^{opt}$ is an estimate of $\mathbf{R}_{rv}$ and $\mathbf{R}^{opt}$ spans the same subspace as $\mathbf{R}_{rv}$. The rank of $\mathbf{R}^{opt}$ is denoted as $r = \text{rank}(\mathbf{R}^{opt})$. By performing SVD, $\mathbf{R}^{opt}$ can be represented as

$$\mathbf{R}^{opt} = \mathbf{U}_o\mathbf{\Sigma}_o\mathbf{V}_o^T.$$

3.4.1. RPCM based DOA estimation

For RPCM, the rank of $\mathbf{R}^{opt}$ reveals the number of the candidate DOAs that satisfy the dual orthogonality (6). Select the columns of $\mathbf{V}_o$ corresponding to the $M_{ca} - r$ zero singular values as the noise subspace, denoted as $\widehat{\mathbf{V}}_n$, we form the real-valued MUSIC spectra as

$$P(\theta) = \frac{1}{\mathbf{a}_{ca}^H(\theta)\widehat{\mathbf{V}}_n\widehat{\mathbf{V}}_n^T\mathbf{a}_{ca}(\theta)}. \tag{28}$$

Due to the dual orthogonality (6), both $\mathbf{a}_{ca}(\theta)$ and $\mathbf{a}_{ca}(-\theta)$ are orthogonal to the noise subspace $\widehat{\mathbf{V}}_n$. Therefore, we just need to search over a half of the total angular field (e.g., $\left[-\frac{\pi}{2}, 0\right]$ or $\left[0, \frac{\pi}{2}\right]$) to locate $\left\lceil\frac{r}{2}\right\rceil$ peaks, and the rest can be recovered according to mirror property.

Then we need to distinguish the true DOAs from the r candidate DOAs. For simplicity, a classical beamforming approach (CBF) [22] is adopted,[1] and the CBF spectra is given as $P_{CBF}(\theta) = \mathbf{a}_{ca}^H(\theta)\mathbf{R}_{sm}\mathbf{a}_{ca}(\theta)$. Notice that $P_{CBF}(\theta)$ corresponding to true DOAs are much larger than those associated with their corresponding symmetrical mirror DOAs. Thus for arbitrary angle $\widehat{\theta}_i (i = 1, 2, \ldots, \left\lceil\frac{r}{2}\right\rceil)$ estimated by (28), we have the following criterion

- When $P_{CBF}(\widehat{\theta}_i) > P_{CBF}(-\widehat{\theta}_i)$, $\widehat{\theta}_i$ is the true DOA.
- When $P_{CBF}(-\widehat{\theta}_i) > P_{CBF}(\widehat{\theta}_i)$, $-\widehat{\theta}_i$ is the true DOA.
- When $P_{CBF}(\widehat{\theta}_i) = P_{CBF}(-\widehat{\theta}_i)$, both $\widehat{\theta}_i$ and $-\widehat{\theta}_i$ are true.

For clarity, we summarize the RPCM based DOA estimation methods in Algorithm 1.

Algorithm 1: Real part of covariance matrix (RPCM) based DOA estimation.

Input : Received signal $\{\mathbf{x}(t)\}_{t=1}^T$
Output: The estimate of $\mathbf{\Theta} = [\theta_1, \theta_2, \ldots, \theta_K]$
Initialization: $p, \rho \in (0, 1)$, η, $\varepsilon^{(0)} > 0$, $\mathbf{w}^{(0)} \leftarrow \mathbf{0}$, and $k \leftarrow 0$;
$\widehat{\mathbf{R}}_{xx} \leftarrow \frac{1}{T}\sum_{t=1}^T \mathbf{x}(t)\mathbf{x}^H(t)$, and compute $\mathbf{R}_{sm}$ as (4);
Take the real part: $\mathbf{R}_{rv}^{(1)} \leftarrow \text{Re}(\mathbf{R}_{sm})$;
repeat
  Update $\widehat{\mathbf{R}}^{(k+1)}$ as (24);
  Update $w_m^{(k+1)} \leftarrow \left(\sigma_m\left(\widehat{\mathbf{R}}^{(k+1)}\right) + \varepsilon^{(k)}\right)^{p-1}$;
  $\varepsilon^{(k)} \leftarrow \rho\varepsilon^{(k-1)}$, $k \leftarrow k+1$;
until $\left\|\widehat{\mathbf{R}}^{(k+1)} - \widehat{\mathbf{R}}^{(k)}\right\|_F < \zeta$;
$\mathbf{R}^{opt} \leftarrow \widehat{\mathbf{R}}^{(k)}$ and its SVD is: $\mathbf{R}^{opt} = \mathbf{U}_o\mathbf{\Sigma}_o\mathbf{V}_o^T$;
$r \leftarrow \text{rank}(\mathbf{R}^{opt})$ and select $M_{ca} - r$ columns of $\mathbf{V}_o$ with respect to zero singular values as the noise subspace;
Compute the MUSIC spectrum $P(\theta)$ (28) and locate the maximum $\left\lceil\frac{r}{2}\right\rceil$ peaks in half angular field $\left[-\frac{\pi}{2}, 0\right]$ or $\left[0, \frac{\pi}{2}\right]$;
Compute the CBF spectrum $P_{CBF}(\theta)$ and determine the true DOAs according to their CBF values.

3.4.2. UTCM based DOA estimation

For UTCM, the rank of $\mathbf{R}^{opt}$ reveals the number of the sources. Select the columns of $\mathbf{V}_o$ corresponding to the $M_{ca} - r$ zero singular values as the noise subspace, denoted as $\widehat{\mathbf{V}}_n$, we form the real-valued MUSIC spectra as

$$P(\theta) = \frac{1}{\underline{\mathbf{a}}_{ca}^T(\theta)\widehat{\mathbf{V}}_n\widehat{\mathbf{V}}_n^T\underline{\mathbf{a}}_{ca}(\theta)}, \tag{29}$$

where $\underline{\mathbf{a}}_{ca}(\theta)$ is the equivalent real-valued steering vector due to unitary transformation, and is defined as

$$\underline{\mathbf{a}}_{ca}(\theta) = \sqrt{2} \times \begin{cases} \left[\cos\left(\frac{M_{ca}-1}{2}\phi\right), \ldots, \cos\left(\frac{1}{2}\phi\right), \sin\left(\frac{1}{2}\phi\right), \right. \\ \qquad \left. \ldots, \sin\left(\frac{M_{ca}-1}{2}\phi\right)\right]^T, \ M_{ca} \text{ is even} \\ \left[\cos\left(\frac{M_{ca}-1}{2}\phi\right), \ldots, \cos(\phi), 1, \sin(\phi), \right. \\ \qquad \left. \ldots, \sin\left(\frac{M_{ca}-1}{2}\phi\right)\right]^T, \ M_{ca} \text{ is odd} \end{cases} \tag{30}$$

and $\phi = \pi\sin\theta$.

The DOAs are estimated by locating the r peaks of the real-valued spectrum $P(\theta)$. For clarity, we summarize the UTCM based DOA estimation methods in Algorithm 2.

[1] Except for the CBF approach, some other methods can also be used, such as the MUSIC and Capon approaches. However, the MUSIC require the SVD of the complex-valued covariance matrix and the Capon needs its inverse operation, which have a heavy computation burden. In this paper, we use the CBF approach for simplicity.

Algorithm 2: Unitary transformation of covariance matrix (UTCM) based DOA estimation.

Input : Received signal $\{\mathbf{x}(t)\}_{t=1}^{T}$
Output: The estimate of $\boldsymbol{\Theta} = [\theta_1, \theta_2, \ldots, \theta_K]$
Initialization: $p, \rho \in (0,\ 1)$, η, $\varepsilon^{(0)} > 0$, $\mathbf{w}^{(0)} \leftarrow \mathbf{0}$, and $k \leftarrow 0$;
$\widehat{\mathbf{R}}_{xx} \leftarrow \frac{1}{T}\sum_{t=1}^{T}\mathbf{x}(t)\mathbf{x}^H(t)$, and compute $\mathbf{R}_{sm}$ as (4);
Unitary transformation: $\mathbf{R}_{rv} \leftarrow \mathrm{Re}\left(\mathbf{Q}_{M_{ca}}\mathbf{R}_{sm}\mathbf{Q}_{M_{ca}}^H\right)$;
repeat
  Update $\widehat{\mathbf{R}}^{(k+1)}$ as(24);
  Update $w_m^{(k+1)} \leftarrow \left(\sigma_m\left(\widehat{\mathbf{R}}^{(k+1)}\right) + \varepsilon^{(k)}\right)^{p-1}$;
  $\varepsilon^{(k)} \leftarrow \rho\varepsilon^{(k-1)}$, $k \leftarrow k+1$;
until $\left\|\widehat{\mathbf{R}}^{(k+1)} - \widehat{\mathbf{R}}^{(k)}\right\|_F < \zeta$;
$\mathbf{R}^{opt} \leftarrow \widehat{\mathbf{R}}^{(k)}$ and its SVD is: $\mathbf{R}^{opt} = \mathbf{U}_o\boldsymbol{\Sigma}_o\mathbf{V}_o^T$;
$r \leftarrow \mathrm{rank}(\mathbf{R}^{opt})$ and select $M_{ca} - r$ columns of $\mathbf{V}_o$ with respect to zero singular values as the noise subspace;
Compute the real-valued MUSIC spectrum $P(\theta)$ (29) and locate the maximum r peaks as the estimates of DOAs.

3.4.3. Complexity analysis

Here we compare the complexities of the proposed RPCM and UTCM approaches with that of the LRD approach. The complexities of the three methods are mainly caused by the low rank matrix recovery step and MUSIC based estimation step.

- *The low rank matrix recovery step*: For RPCM and UTCM, the SVD of a real-valued matrix is necessary, which requires $\mathcal{O}(M_{ca}^3)$ real-valued multiplications [23]. Then the update of $\mathbf{R}$ and $\mathbf{w}$ requires $\mathcal{O}(M_{ca}^3 + M_{ca}^2)$ and $\mathcal{O}(M_{ca}^3)$ real-valued multiplications, respectively. Let L_1 and L_2 denote the iteration times for RPCM and UTCM, then the complexities can be given as $\mathcal{O}\left(L_1(2M_{ca}^3 + M_{ca}^2)\right)$ and $\mathcal{O}\left(L_2(2M_{ca}^3 + M_{ca}^2)\right)$, respectively. The LRD approach uses the singular value thresholding approach [24] to recover the complex-valued covariance matrix, which mainly requires $4 \times \mathcal{O}\left(L_3(2M_{ca}^3 + M_{ca}^2)\right)$ real-valued multiplications [25], and L_3 denotes the iteration times for LRD. As the iterative approach of LRD mainly involves complex-valued operations, $L_3 > L_1$, L_2 holds as a result.
- *MUSIC based estimation step*: Computing SVD to obtain the noise subspace requires $\mathcal{O}(M_{ca}^3)$ and $4 \times \mathcal{O}(M_{ca}^3)$ real-valued operations for the real- and complex-valued covariance matrices, respectively. To compute the MUSIC spectrum, $\mathcal{O}(J(M_{ca}+1)(M_{ca}-K))$ is involved for UTCM, where J denote the total sample points over $\left[-\frac{\pi}{2}, \frac{\pi}{2}\right]$. As RPCM can halve the spectral search region and the steering vector $\mathbf{a}_{ca}^H$ is complex, the complexity for spectral search is $2 \times \mathcal{O}\left(\frac{J}{2}(M_{ca}+1)(M_{ca}-2K)\right)$. Moreover, to distinguish the true and mirror angles requires $\mathcal{O}(2K(M_{ca}+1)(M_{ca}-2K))$ real-valued operations for PRCM. For LRD, the complexity of spectral search is given as $4 \times \mathcal{O}(J(M_{ca}+1)(M_{ca}-K))$.

Overall, the complexities for UTCM, PRCM, and LRD are given respectively as

$$\mathcal{C}_{UTCM} = \mathcal{O}\left(L_1(2M_{ca}^3 + M_{ca}^2)\right) + \mathcal{O}(M_{ca}^3) + \mathcal{O}(J(M_{ca}+1)(M_{ca}-K)), \tag{31}$$

$$\begin{aligned}\mathcal{C}_{RPCM} = {} & \mathcal{O}\left(L_2(2M_{ca}^3 + M_{ca}^2)\right) + \mathcal{O}(M_{ca}^3) + 2 \\ & \times\mathcal{O}\left(\frac{J}{2}(M_{ca}+1)(M_{ca}-2K)\right) \\ & + \mathcal{O}(2K(M_{ca}+1)(M_{ca}-2K)),\end{aligned} \tag{32}$$

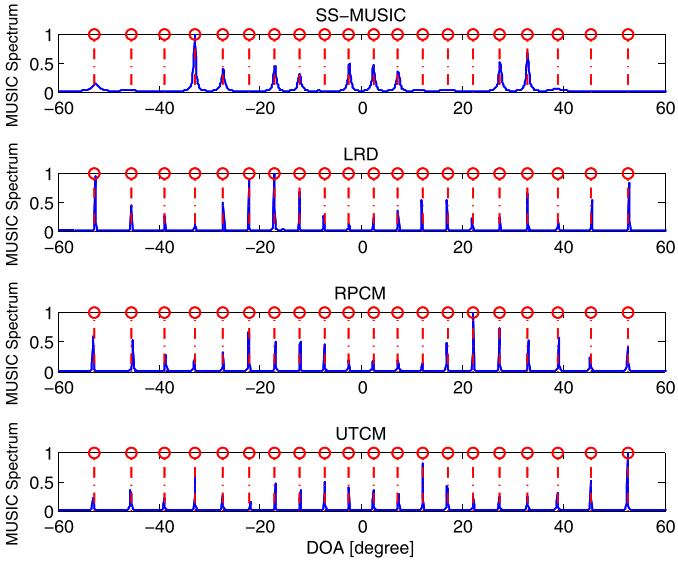

Fig. 1. Normalized spectra of the four methods for nested MRA with $K = 20$, $T = 500$, and $SNR = 0$ dB. The dashed lines denote the true DOAs.

and

$$\begin{aligned}\mathcal{C}_{LRD} = {} & 4 \times \left(\mathcal{O}\left(L_3(2M_{ca}^3 + M_{ca}^2)\right)\right. \\ & \left. + \mathcal{O}(M_{ca}^3) + \mathcal{O}(J(M_{ca}+1)(M_{ca}-K))\right)\end{aligned} \tag{33}$$

As can be observed, both UTCM and RPCM can substantially reduce the computational complexities, since they can reduce the participation of complex-valued operations.

4. Performance evaluation

In this section, we use simulation results to validate the effectiveness of the proposed algorithm. We consider two types of array geometries, i.e., MRA [6] and nested MRA [11] with $M = 12$ sensors. The sensors of the MRA geometry are non-uniformly located at positions $[0, 1, 6, 14, 22, 30, 38, 40, 42, 45, 47, 49]\frac{\lambda}{2}$, while the sensors are located at $[0, 1, 4, 6, 13, 14, 17, 19, 39, 40, 43, 45]\frac{\lambda}{2}$ for the nested MRA. We compare the proposed algorithm with spatial smoothing-MUSIC (SS-MUSIC) [7] and the LRD approach [12]. Since SS-MUSIC requires the source number K *a priori*, we use the predicted eigen-threshold approach [26] to estimate K. The following parameters are used for the proposed algorithms: $p = 0.2$, $\rho = 0.6$, $\eta = 10$, and $\varepsilon^{(0)} = 0.1$.

4.1. Experiment 1: Comparison of detectable capability

We first compare the detectable capability of the four methods with MRA and nested MRA geometries, respectively. We consider $K = 20 > M$ narrowband sources impinging on the array from DOAs uniformly distributed within the range from -55° to 55°, which is more than the number of physical sensors. Figs. 1 and 2 depicts the normalized MUSIC spectrum for the nested MRA and MRA, respectively, where $T = 500$ and $SNR = 0$ dB. The true DOAs are represented by dashed lines. It is observed that LRD, the proposed RPCM and UTCM methods can detect all the sources successfully, while SS-MUSIC only resolves some of them. Thus, the proposed methods are superior to SS-MUSIC. Meanwhile, as compared to LRD, the proposed method can reduce the participation of complex-valued operations and can reduce the complexity substantially, which will be verified later.

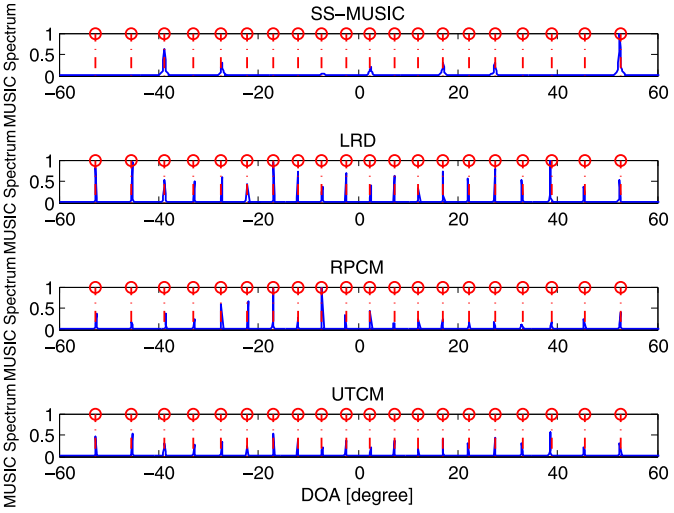

Fig. 2. Normalized spectra of the four methods for MRA with $K = 20$, $T = 500$, and $SNR = 0$ dB. The dashed lines denote the true DOAs.

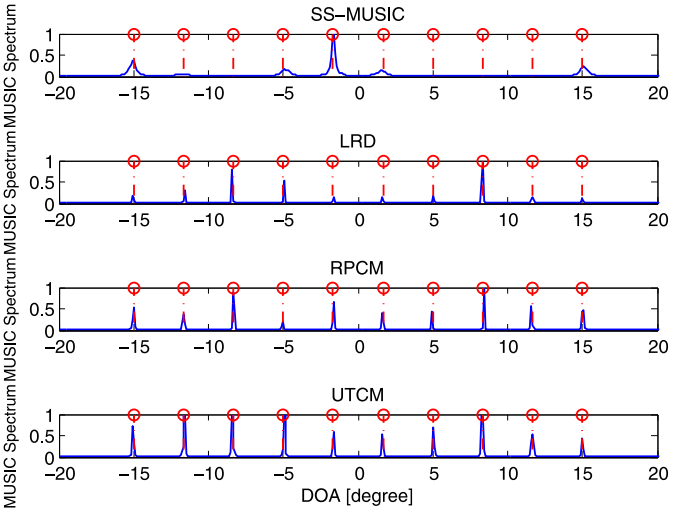

Fig. 3. Normalized spectra of the four methods for nested MRA with $K = 10$, $T = 500$, and $SNR = 0$ dB. The dashed lines denote the true DOAs.

4.2. Experiment 2: Comparison of resolution ability

To investigate the resolution ability, we consider $K = 10$ closely-located sources, which are uniformly distributed within the range from -15° to 15°. Figs. 3 and 4 shows the normalized MUSIC spectrum of the 10 closely-located sources for the nested MRA and MRA, respectively, where $T = 500$ and $SNR = 0$ dB. As can be observed, LRD, RPCM and UTCM can successfully resolve all these closely-located sources, while SS-MUSIC fails. Therefore, the proposed methods outperform SS-MUSIC when resolving closely-located sources. Meanwhile, the proposed methods are superior to LRD due to the reduced complexity.

4.3. Experiment 3: Comparison of estimation accuracy

We then compare the estimation performance of the four methods in terms of root mean square error (RMSE). Figs. 5 and 6 depict the RMSE performance versus signal-to-noise ratio (SNR) for nested MRA and MRA, respectively, where $T = 500$. Figs. 7 and 8 show the RMSE performance against the number of snapshots with $SNR = 0$ dB for nested MRA and MRA, respectively. As is shown, the estimation performance is improved with the increase of SNR and

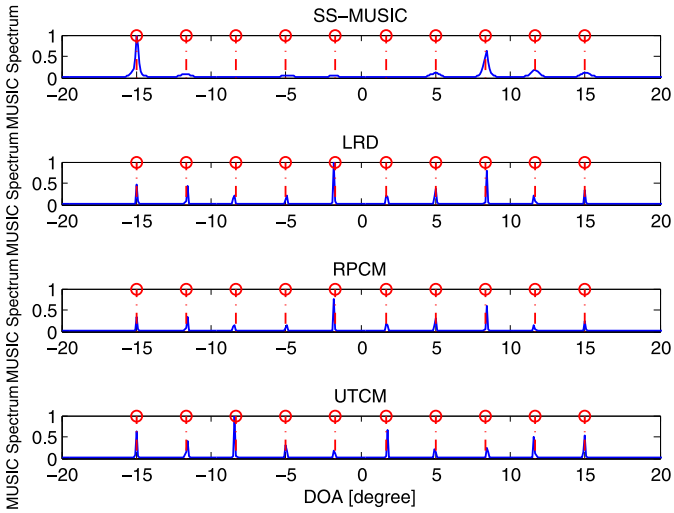

Fig. 4. Normalized spectra of the four methods for MRA with $K = 10$, $T = 500$, and $SNR = 0$ dB. The dashed lines denote the true DOAs.

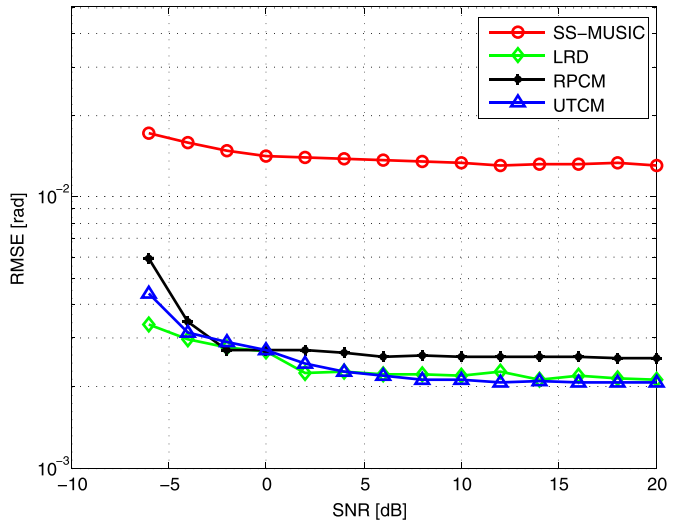

Fig. 5. RMSE versus SNR for the nested MRA with $M = 12$, $K = 20$, and $T = 500$.

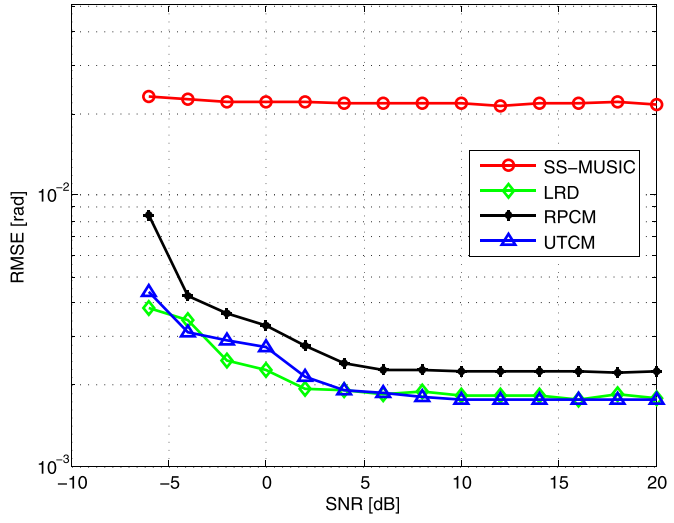

Fig. 6. RMSE versus SNR for MRA with $M = 12$, $K = 20$, and $T = 500$.

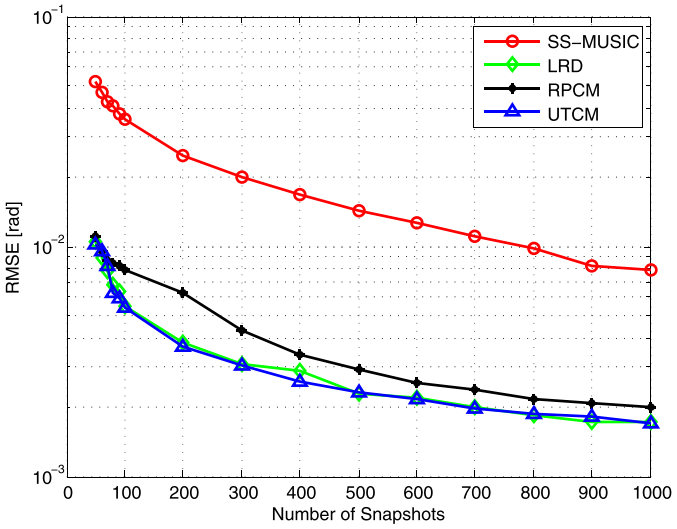

Fig. 7. RMSE versus snapshots number for the nested MRA with $M = 12$, $K = 20$, and $SNR = 0$ dB.

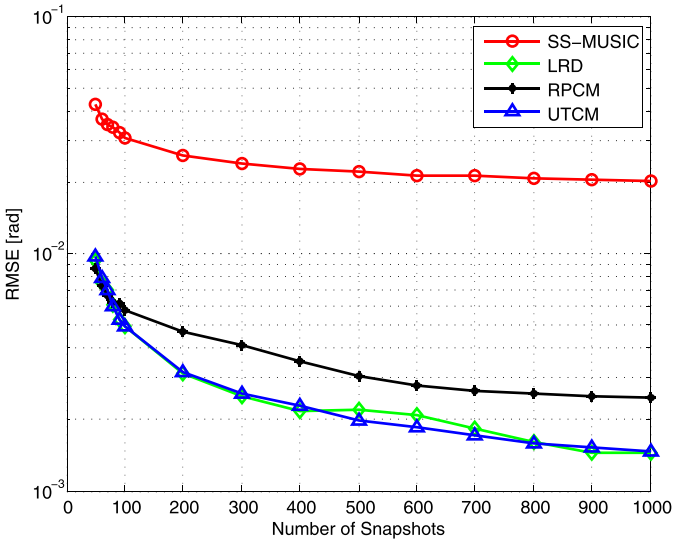

Fig. 8. RMSE versus snapshots number for MRA with $M = 12$, $K = 20$, and $SNR = 0$ dB.

snapshot number, as more accurate covariance matrix can be obtained for larger SNR and more samples. The LRD and the two proposed methods outperform SS-MUSIC greatly, which suffers from the inaccurate source number information caused by the predicted eigen-threshold approach [26]. As compared to LRD, the proposed UTCM based approach can provide almost the same estimation performance, while the proposed RPCM approach is slightly worse than LRD. This is because that RPCM only utilizes part of the covariance matrix, which leads to information loss as a result. Notice that the proposed methods can substantially reduce the participation of complex-valued operations and/or halve the spectral search region, thus, the proposed methods are more efficient than LRD.

4.4. Experiment 4: Comparison of CPU time

Finally, the average CPU time is provided in Table 1 for comparison. As can be observed, the two proposed methods have comparable CPU run time as SS-MUSIC, but provide much better estimation accuracy. As compared to LRD, the proposed methods can achieve almost the same performance, while the CPU run time is substantially reduced. This is because that the proposed methods can utilize the real-valued covariance matrix to estimate DOAs and the proposed reweighted nuclear norm minimization approach can converge within a few iterations, which will reduce the complexity greatly as compared to its complex-valued version. In this respective, the proposed methods provide the best accuracy-complexity tradeoff, which is quite attractive, especially for larger M.

Table 1
CPU time of SS-MUSIC, LRD, RPCM and UTCM.

Algorithms	$M = 9$	$M = 12$	$M = 21$
SS-MUSIC	0.82 s	1.07 s	1.45 s
LRD	8.34 s	32.6 s	98.9 s
RPCM	1.21 s	1.48 s	2.72 s
UTCM	0.37 s	0.69 s	1.02 s

5. Conclusion

In this work, we have proposed two novel real-valued DOA estimation methods without knowing the number of sources via reweighted nuclear norm minimization. The complex-valued covariance matrix is firstly converted as a real-valued one via unitary transformation or taking the real (or imaginary) part. Then a real-valued low rank recovery problem is proposed to reveal the number of sources, which can be solved efficiently. The advantage of the proposed methods is that the involved low rank recovery, SVD and spectral search steps mainly requires real-valued operations and therefore reduce the complexity greatly. Simulation results have shown that the proposed methods can provide superior estimation accuracy with substantially reduced complexity.

Acknowledgments

This work was supported by the National Natural Science Foundation of China [grant number 61501510, 61631020, and 61601504] and Shandong Provincial Natural Science Foundation, China [grant number ZR2017PF007 and ZR2016FB19].

References

[1] H. Krim, M. Viberg, Two decades of array signal processing research: the parametric approach, IEEE Signal Process. Mag. 13 (4) (1996) 67–94, doi:10.1109/79.526899.
[2] J. Capon, High-resolution frequency–wavenumber spectrum analysis, Proc. IEEE 57 (8) (1969) 1408–1418, doi:10.1109/PROC.1969.7278.
[3] R. Schmidt, Multiple emitter location and signal parameter estimation, IEEE Trans. Antennas Propag. 34 (3) (1986) 276–280, doi:10.1109/TAP.1986.1143830.
[4] R. Roy, T. Kailath, Esprit-estimation of signal parameters via rotational invariance techniques, IEEE Trans. Acoust. Speech Signal Process. 37 (7) (1989) 984–995, doi:10.1109/29.32276.
[5] B.D. Rao, K.V.S. Hari, Performance analysis of root-music, IEEE Trans. Acoust. Speech Signal Process. 37 (12) (1989) 1939–1949, doi:10.1109/29.45540.
[6] M. Ishiguro, Minimum redundancy linear arrays for a large number of antennas, Radio Sci. 15 (06) (1980) 1163–1170, doi:10.1029/RS015i006p01163.
[7] P. Pal, P.P. Vaidyanathan, Coprime sampling and the music algorithm, in: Digital Signal Processing Workshop and IEEE Signal Processing Education Workshop (DSP/SPE), 2011 IEEE, 2011, pp. 289–294, doi:10.1109/DSP-SPE.2011.5739227.
[8] F. Sun, P. Lan, B. Gao, Partial spectral search-based doa estimation method for co-prime linear arrays, Electron. Lett. 51 (24) (2015) 2053–2055, doi:10.1049/el.2015.2261.
[9] P. Pal, P.P. Vaidyanathan, Nested arrays: a novel approach to array processing with enhanced degrees of freedom, IEEE Trans. Signal Process. 58 (8) (2010) 4167–4181, doi:10.1109/TSP.2010.2049264.
[10] C.L. Liu, P.P. Vaidyanathan, Super nested arrays: Linear sparse arrays with reduced mutual coupling part i: fundamentals, IEEE Trans. Signal Process. 64 (15) (2010) 3997–4012, doi:10.1109/TSP.2016.2558159.
[11] M. Yang, A.M. Haimovich, B. Chen, X. Yuan, A new array geometry for doa estimation with enhanced degrees of freedom, in: 2016 IEEE International Conference on Acoustics, Speech and Signal Processing (ICASSP), 2016, pp. 3041–3045, doi:10.1109/ICASSP.2016.7472236.
[12] P. Pal, P.P. Vaidyanathan, A grid-less approach to underdetermined direction of arrival estimation via low rank matrix denoising, IEEE Signal Process. Lett. 21 (6) (2014) 737–741, doi:10.1109/LSP.2014.2314175.

[13] C. Liu, P.P. Vaidyanathan, P. Pal, Coprime coarray interpolation for doa estimation via nuclear norm minimization, in: 2016 IEEE International Symposium on Circuits and Systems (ISCAS), 2016, pp. 2639–2642, doi:10.1109/ISCAS.2016.7539135.
[14] Y.D. Zhang, M.G. Amin, B. Himed, Sparsity-based doa estimation using co-prime arrays, in: 2013 IEEE International Conference on Acoustics, Speech and Signal Processing, 2013, pp. 3967–3971, doi:10.1109/ICASSP.2013.6638403.
[15] P. Pal, P.P. Vaidyanathan, Correlation-aware sparse support recovery: Gaussian sources, in: 2013 IEEE International Conference on Acoustics, Speech and Signal Processing, 2013, pp. 5880–5884, doi:10.1109/ICASSP.2013.6638792.
[16] F. Yan, M. Jin, S. Liu, X. Qiao, Real-valued music for efficient direction estimation with arbitrary array geometries, IEEE Trans. Signal Process. 62 (6) (2014) 1548–1560, doi:10.1109/TSP.2014.2298384.
[17] J. Li, D. Jiang, X. Zhang, Doa estimation based on combined unitary esprit for coprime mimo radar, IEEE Commun. Lett. 21 (1) (2017) 96–99, doi:10.1109/LCOMM.2016.2618789.
[18] F. Sun, Q. Wu, Y. Sun, G. Ding, P. Lan, An iterative approach for sparse direction-of-arrival estimation in co-prime arrays with off-grid targets, Digital Signal Process. 61 (2017) 35–42, doi:10.1016/j.dsp.2016.06.007.
[19] J. Dai, W. Xu, D. Zhao, Real-valued doa estimation for uniform linear array with unknown mutual coupling, Signal Process. 92 (9) (2012) 2056–2065, doi:10.1016/j.sigpro.2012.01.017.
[20] X. Lin, G. Wei, Accelerated reweighted nuclear norm minimization algorithm for low rank matrix recovery, Signal Process. 114 (2015) 24–33, doi:10.1016/j.sigpro.2015.02.004.
[21] L. Mirsky, A trace inequality of John von Neumann, Monatsh. Math. 79 (4) (1975) 303–306, doi:10.1007/BF01647331.
[22] D.H. Johnson, D.E. Dudgeon, Array Signal Processing: Concepts and Techniques, Prentice Hall, 1993.
[23] G.H. Golub, C.F.V. Loan, Matrix Computations, JHU Press, 2012.
[24] J. Cai, E. Candes, Z. Shen, A singular value thresholding algorithm for matrix completion, SIAM J. Optim. 20 (4) (2008) 1956–1982, doi:10.1137/080738970.
[25] J. Cai, S. Osher, Fast singular value thresholding without singular value decomposition, Methods Appl. Anal. 20 (4) (2013) 335–352, doi:10.4310/MAA.2013.v20.n4.a2.
[26] W. Chen, K.M. Wong, J.P. Reilly, Detection of the number of signals: a predicted eigen-threshold approach, IEEE Trans. Signal Process. 39 (5) (1991) 1088–1098, doi:10.1109/78.80959.